



Study of the mechanochemical process to crystalline $\text{Cu}_2\text{ZnSnS}_4$ powder



Anna Ritscher^{a,b}, Marc Schlosser^c, Arno Pfitzner^c, Martin Lerch^{a,*}

^a Institut für Chemie, Technische Universität Berlin, Straße des 17. Juni 135, 10623 Berlin, Germany

^b Helmholtz-Zentrum Berlin für Materialien und Energie, Abteilung Kristallographie, Hahn-Meitner-Platz 1, 14109 Berlin, Germany

^c Institut für Anorganische Chemie, Universität Regensburg, Universitätsstr. 31, 93040 Regensburg, Germany

ARTICLE INFO

Article history:

Received 17 May 2016

Received in revised form 26 July 2016

Accepted 5 August 2016

Available online 6 August 2016

Keywords:

- A. Semiconductors
- B. Chemical synthesis
- C. X-ray diffraction
- D. Crystal structure
- D. Defects

ABSTRACT

Kesterite-type $\text{Cu}_2\text{ZnSnS}_4$ was synthesized from the corresponding binary sulfides by a mechanochemical route in a planetary ball mill. The reaction progress during this milling step was followed within a time range of 10–180 min by powder X-ray diffraction. In addition, the crystallization of the milled material was studied *in situ* by high-temperature X-ray diffraction methods in the temperature range of 300–500 °C. Significant disorder (cation distribution) was observed at 500 °C, strongly decreasing during cooling down to ambient temperature with a rate of 60 K/h.

© 2016 Elsevier Ltd. All rights reserved.

1. Introduction

Systematic analysis of the semiconductor compound $\text{Cu}_2\text{ZnSnS}_4$ (CZTS) and its structural, chemical, and physical properties have been in the focus of interest in the last few years [1–6]. This quaternary chalcogenide exhibits a great potential as absorber material for applications in thin film photovoltaics. Due to its suitable properties (optical band gap energy = 1.5 eV, absorption coefficient in the order of 10^{-4}cm^{-1} [7–9]) this material is discussed as a promising low-cost alternative to In-containing $\text{CuIn}_x\text{Ga}_{(1-x)}\text{Se}_2$ (CIGS). The current record efficiency of 12.6% was reached for CZTS-based devices containing additional selenium [10].

After some controversies about the correct crystal structure of $\text{Cu}_2\text{ZnSnS}_4$ it was demonstrated in different studies that this quaternary sulfide adopts the kesterite structure type (space group $\bar{I}4$) [11,12]. This tetragonal crystal structure derives from the sphalerite structure type (known for ZnS etc.) by doubling the c-axis and it consists of alternating cation layers stacked along this axis (see Fig. 1).

The lattice planes at $z=0$ and $z=1/2$ are occupied by Cu and Sn in an ordered manner, i.e. Cu is found on Wyckoff position 2a (0, 0, 0) and Sn on position 2b (0, 0, 1/2). Remaining Cu and Zn atoms are

located on lattice planes at $z=1/4$ and $z=3/4$, position 2c (0, 1/2, 1/4) and 2d (0, 1/2, 3/4), respectively. *Ab initio* calculations [13,14] showed that, due to its very low formation energy, the point defect complex ($\text{Cu}_{\text{Zn}} + \text{Zn}_{\text{Cu}}$) is easily formed and thus Cu/Zn disorder has to be expected. This was also confirmed by diffraction studies on CZTS powder samples, where partial [15,16] or complete disorder [1] of Cu and Zn on the 2c and 2d positions was reported.

High temperature X-ray diffraction measurements of kesterite powder using synchrotron radiation show that $\text{Cu}_2\text{ZnSnS}_4$ undergoes a structural phase transition from the tetragonal kesterite- to the cubic sphalerite-type structure at temperatures above of 866 °C [2]. The transition leads to a random distribution of the cations Cu, Zn, and Sn (space group $F\bar{4}3m$). Due to the formation of secondary phases it is challenging to prepare phase-pure CZTS powder, which is important for detailed studies concerning the correlations between structural and electronic properties. Bulk material of CZTS has been usually produced by solid state reaction of the elements in evacuated silica ampoules [1,17]. Due to the high sulfur vapor pressure it is necessary to apply a well-defined temperature program and homogenization is achieved by a second annealing step at 750 °C. All these factors result in long reaction times and an enhanced possibility for the formation of secondary phases.

Recently we presented an easy and fast process for the preparation of single phase CZTS powders [16]. The main idea was the development of a synthesis route at temperatures significantly lower than 750 °C. This was realized by a

* Corresponding author at:

E-mail address: martin.lerch@tu-berlin.de (M. Lerch).

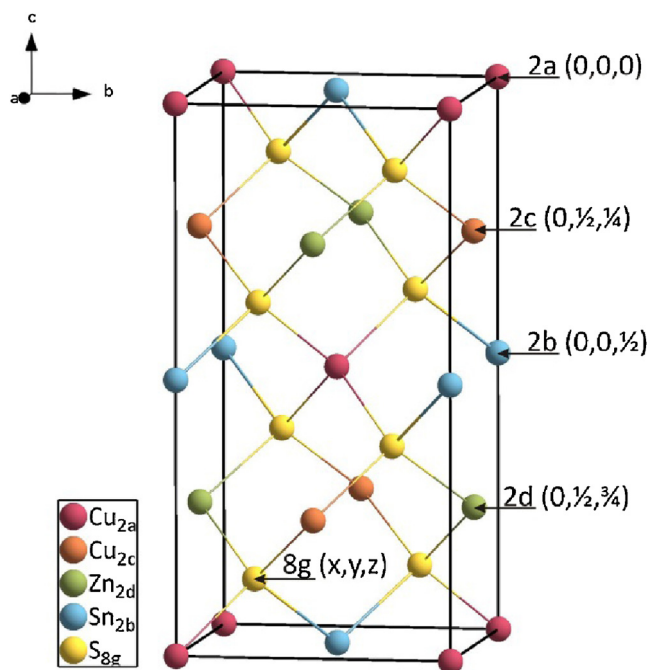


Fig. 1. Unit cell of fully ordered kesterite-type $\text{Cu}_2\text{ZnSnS}_4$, all occupied Wyckoff positions are labeled.

mechanochemical approach and the synthesis of a precursor by reaction of the corresponding binary sulfides CuS , ZnS , and SnS in a planetary ball mill. Mechanochemical processes in planetary ball mills find a widespread use in science and industry due to the feasibility of rapid, highly efficient and usually solvent-free chemical synthesis. Additionally, it is possible to develop compounds that cannot be obtained via a conventional solid-state route [18].

After annealing at 500°C in a H_2S atmosphere, a highly crystalline product is obtained. A similar mechanochemical process was reported in Ref. [19], where $\text{Cu}_2\text{ZnSnX}_4$ ($X=\text{S}, \text{Se}$) bulk material was prepared in a ball mill starting from the metals and the chalcogens.

In this contribution we present a more detailed study of our new two-step synthesis process. The reaction process in the ball mill as function of time as well as the crystallization behavior of the poorly crystalline CZTS precursor to the crystalline powder with temperature are investigated.

2. Experimental

Sulfide powders with the chemical formula $\text{Cu}_2\text{ZnSnS}_4$ were prepared by our mechanical process [16]. CuS , ZnS , and SnS were mixed in a molar ratio of 2:1:1 without any additional fluid medium and filled into an 80 ml agate jar (including 5 grinding balls with a diameter of 20 mm). Milling was performed in a Fritsch Planetary Mono Mill PULVERISETTE 6 using a rotational speed of 400 rpm and milling times of up to 180 min. Small amounts of the sample were withdrawn at time intervals of 10–30 min for diffraction analyses.

In order to get a highly crystalline product as reference, one half of the as-milled powder (milling time 180 min) was annealed in a conventional tube furnace equipped with a SiO_2 -tube in H_2S -atmosphere for 3 h at 500°C . After this treatment, the sample was cooled down with a rate of 60 K/h. X-ray powder diffraction was used for the structural characterization of all samples. Diffraction data

were collected using a Panalytical X'Pert PRO diffractometer (Bragg-Brentano geometry, $\text{Cu-K}\alpha$ radiation). Structural refinements were performed by the Rietveld method [20] with the program package Fullprof Suite Version 2015 [21] by applying a pseudo-Voigt function. The kesterite-type structure (space group $\bar{1}4$) was used as starting model for the refinement.

The second half of the sample was used for the investigation of the crystallization behavior of the quaternary sulfide precursor by *in situ* high-temperature X-ray diffraction with the help of a STOE STADI P diffractometer (Transmission/Debye Scherrer geometry, $\text{Mo-K}\alpha_1$ radiation). The instrument was equipped with a STOE furnace using a Ni/CrNi thermocouple. The sample was encapsulated in an evacuated silica capillary and initially measured at room temperature (RT, measurement number 001). Then the sample was heated to 300°C with a rate of 50 K/min and subsequently measured at 300°C every 10 min in order to follow the isothermal phase formation and growth of the crystallites (20 measurements, 1 min, measurement numbers $N=002$ –021). Afterwards, the temperature was raised to 400°C and the powder was again measured every 10 min (measurement numbers $N=022$ –042). A further heating step up to a temperature of 500°C was applied (measurement numbers $N=043$ –062). Again diffraction patterns were recorded every 10 min. As a reference measurement a diffraction pattern of the empty furnace without any sample was recorded in order to detect the signals from the furnace (measurement number $N=000$).

3. Results and discussion

As described in the experimental section, the first synthesis step to phase pure $\text{Cu}_2\text{ZnSnS}_4$ powder is the reaction of the corresponding binary sulfides (CuS , ZnS , SnS) in a ball mill. In order to follow this reaction process, small amounts of powder were withdrawn from the grinding bowl by interrupting the milling procedure several times. Fig. 2 depicts the XRD patterns of the prepared CZTS powders milled for 10–180 min.

Up to a milling time of 30 min the reflections originating from the binary sulfides are the main signals in the diffraction patterns. During this early stage of milling, the powders of CuS , ZnS , and SnS are mixed together and no reaction takes place. After 40 min of milling the intensities of the reflections that can be assigned to the

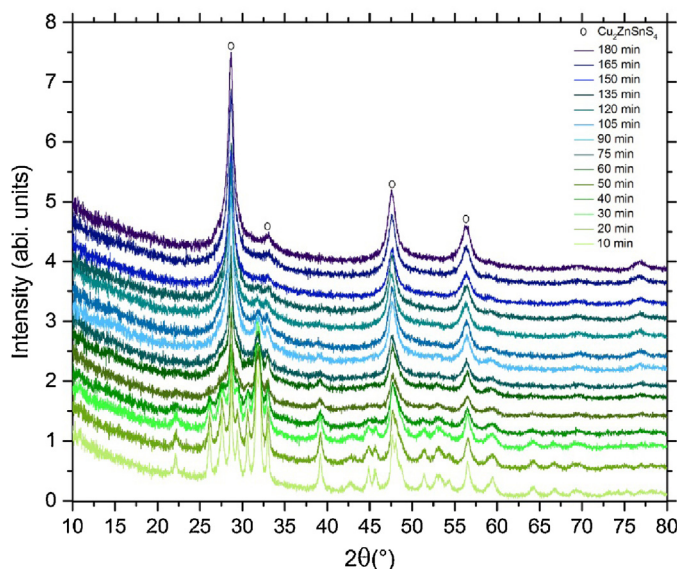


Fig. 2. Diffraction patterns ($\text{Cu-K}\alpha$ radiation) of as-prepared samples after the milling process at different times ($t=10$ –180 min).

binary compounds begin to decrease, which indicates that the solid-state reaction is activated and the product starts to form, and after 150 min it is clearly seen that the signals have disappeared. The sample was further treated up to a total milling time of 180 min. However, the diffraction pattern did not change significantly, thus at this stage the reaction is considered to be terminated. Taking a look at the change of the reflection position of the major reflection a clear trend to lower 2θ values is visible ($2\theta = 28.68 \rightarrow 28.62$), which is an indication that the quaternary compound is formed during the reaction in the ball mill. The observed reflection positions of the final as-milled powder correspond to the strongest ones expected for the quaternary compound. However, from the obtained X-ray diffraction patterns it is not possible to extract unequivocal information concerning the distribution of the cations as the main reflections of the kesterite phase (partially or fully ordered) practically have the same positions as the expected ones for a sphalerite-type structure (fully disordered) with the same chemical composition. The superlattice reflections for the kesterite-type phase are rather small (see Fig. 4) but their total absence points to severe disorder in the milled material. For more unambiguous results additional investigations, for example by EXAFS, would be necessary.

In addition, as it can be clearly seen in Fig. 2 the milling process results in very broad reflections. The FWHM values increase with increasing milling time as shown in Fig. 3. Profile analyses revealed a dominant Lorentzian shape which can be attributed to crystallite size broadening. The crystallite sizes of the precursor powders are calculated using the Scherrer equation (Eq.(1)) from the strong 112-reflection at $2\theta \sim 28.6^\circ$ [22],

$$\Delta(2\theta) = \frac{K\lambda}{L\cos\theta_0} \quad (1)$$

where $\Delta(2\theta)$ is the line width at half the maximum intensity (FWHM), K is the Scherrer-form factor, in this study a factor of 1 was used, λ is the wavelength, L the mean size of the crystallite, and θ_0 the diffraction angle. $\Delta(2\theta)$ has to be corrected for reflex broadening coming from the instrument according to $\Delta(2\theta) = (\beta_M^2 - \beta_I^2)^{1/2}$ (β_M is measured FWHM and β_I is the correction factor for instrument broadening).

As depicted in Fig. 3, the particle size after 10 min of milling is calculated to 37 nm. In the first 90 min the crystallite size decreases rapidly, approaching a value of about 15 nm. On further milling the crystallite size slightly changes reaching a size of ~ 11 nm after 180 min. In order to confirm the calculated value, TEM

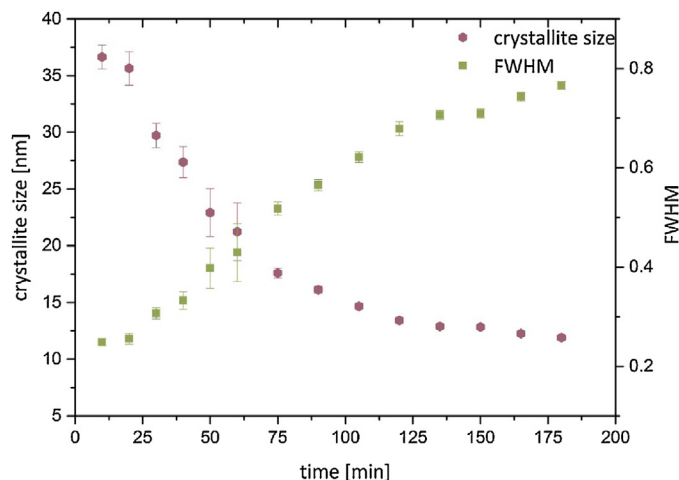


Fig. 3. FWHM values and corresponding crystallite sizes during reaction in the ball mill.

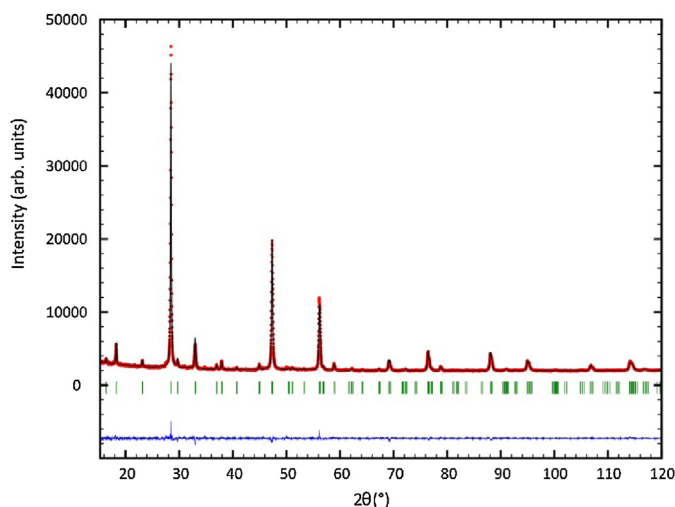


Fig. 4. X-ray powder diffraction pattern with the results of the Rietveld refinement using the kesterite-type structure as starting model.

measurements were carried out with this sample. The observed crystallite sizes were found to be in a range of 8–13 nm which is in good agreement with the result of the Scherrer method (~ 11 nm).

In order to prepare a highly crystalline reference sample, one half of the precursor powder was annealed in a tube furnace (H_2S atmosphere) according to the second step of our mechanochemical process [16]. The structural parameters of the annealed sample were refined (see Tables 1 and 2). As it was shown in our recent studies, it is nicely possible to control the composition of the synthesized powder with the mechanochemical method [16,23]. Therefore, for the structural refinement the ideal composition $\text{Cu}_2\text{ZnSnS}_4$ was used. The X-ray powder diagram with the results of the Rietveld refinement is depicted in Fig. 4.

It should be mentioned that it is not possible to differentiate between Zn and Cu using conventional X-ray powder diffraction methods. Consequently, we can only distinguish between Cu/Zn and Sn. Unfortunately, the amount of prepared material was not sufficient for neutron diffraction experiments. For the refinements, the following side conditions were set: the sum of Cu/Zn on all positions must be 3, the sum of Sn on all positions must be 1, and all four cation positions have to be fully occupied.

Table 2 lists the final atomic and additional structural parameters. As expected, Sn was found on Wyckoff position 2b (0, 0, 1/2), whereas Cu/Zn is located on 2a (0, 0, 0), 2c (0, 1/2, 1/4), and 2d (0, 1/2, 3/4) sites. No Sn is found on position 2c. On 2a and 2d sites very small amounts of Sn (around 1%) are found. Missing Sn on the 2b site is replaced by Cu/Zn. These results are in agreement with our recent refinements [16].

Table 1
Lattice parameters of CZTS and residual values of the Rietveld refinement.

	X-ray diffraction
Structure type	kesterite
Crystal system	tetragonal
Space group	$\bar{4}$ (No.82)
Diffractometer	Panalytical X'Pert PRO
Wavelength α_1, α_2	154.06 pm, 154.44 pm
2θ range	10–120°
a/pm	543.347(13)
c/pm	1083.72(3)
$R_{\text{Bragg}}/\%$	3.84
$R_{\text{wp}}/\%$	2.44
$R_{\text{exp}}/\%$	2.02
S	1.20

Table 2
Refined structural parameters for CZTS from X-ray diffraction.

Atom	Wyckoff	x	y	z	B_{iso}	occ
Cu/Zn	2a	0	0	0	1.88(7)	0.995(2)
Sn	2a	0	0	0	1.88(7)	0.005(2)
Cu/Zn	2c	0	1/2	1/4	0.83(5)	1.000(2)
Sn	2c	0	1/2	1/4	0.83(5)	0.000(2)
Cu/Zn	2d	0	1/2	3/4	0.83(5)	0.989(3)
Sn	2d	0	1/2	3/4	0.83(5)	0.011(3)
Cu/Zn	2b	0	0	1/2	1.15(3)	0.016(2)
Sn	2b	0	0	1/2	1.15(3)	0.984(2)
S	8g	0.7472(12)	0.7612(12)	0.8695(3)	0.48(3)	4

The second half of the as-milled precursor was used to examine the effect of heat treatment on the crystallization of mechanochemically synthesized CZTS powder by *in situ* high-temperature X-ray diffraction. As pointed out in the experimental section, some series of isothermal measurements at 300, 400, and 500 °C were performed. The evolution of the XRD patterns collected during heating is depicted in Fig. 5 and 6. For a first overview, Fig. 5 presents a 3D plot and a rainbow contour plot of all high temperature X-ray patterns.

In order to avoid informational overflow, Fig. 6 (left) presents only one half of measured patterns (including the pattern with signals from the empty furnace), whereas in Fig. 6 (right) the last *in situ* measurement of each annealing temperature (300, 400, 500 °C) as well as the diffraction pattern at 25 °C is shown. It is clearly seen that the reflections of as-milled CZTS became sharper with heating time, indicating increased crystallinity.

As expected, increasing temperature led to a decrease of the full width at half maximum (FWHM) values (see Fig. 7a). The measurement of the starting material (25 °C) gives a calculated crystallite size of 12 nm, which is in good agreement with the result from the diffractometer working with Cu-K α radiation (See Fig. 4).

Having a closer look at the results coming from different annealing temperatures significant differences are found (See Fig. 7b). At 300 °C the crystallization is rather slow, the crystallite sizes barely increase. After 3.5 h sizes of ~15 nm are reached (see Fig. 7b). As expected, a significantly faster increase is observed for 400 °C, where a final size of 37 nm is calculated. In the last annealing step at 500 °C the crystallite size is still increasing and reaches a value of 50 nm after 3.5 h.

As shown in Fig. 7b, the crystallite size increases almost linearly at 400 °C and above.

Using the final data set measured at 500 °C (N = 062), the crystal structure was also refined. The X-ray powder pattern with the results of the Rietveld refinement is depicted in Fig. 8. Lattice

parameters and residual values are summarized in Table 3. As already described above, space group $I\bar{4}$ was used together with additional side conditions as copper and zinc cannot be distinguished by conventional X-ray diffraction methods. Table 4 lists the final atomic and other structural parameters.

Sn is mainly located on Wyckoff position 2b, whereas Cu/Zn is found on the other three cation sites. No significant amount of Sn was found on positions 2a and 2c. In contrast, a significant amount of tin (~8%) was found on the 2d site, whereas missing Sn is replaced by Cu/Zn on 2b. For CZTS it is known that intrinsic defects can be easily formed while the kesterite-type structure (space group $I\bar{4}$) is maintained, e.g. [17,24–26]. Theoretical work [14,27] has shown that the defect cluster $[Zn^{2-}_{sn} + Sn^{2+}_{zn}]$ has relatively low formation energy (around 0.9 eV/pair). Therefore $Sn_{Cu/Zn}$ and Cu/Zn_{Sn} defects should be present when increasing the temperature. Keep in mind that Zn and Cu cannot be distinguished with conventional X-ray diffraction techniques. Consequently, the actual defect clusters in the present sample cannot be determined unequivocally.

The refined values can be compared with the values for the above-presented sample annealed at 500 °C and cooled down with a rate of 60 K/h. At 500 °C, $Sn_{Cu/Zn}$ and Cu/Zn_{Sn} anti-site defects are clearly present; in the sample slowly cooled down to 25 °C hardly any Sn disorder is found. Consequently, it can be presumed that these defects heal out rapidly during cooling down to ambient temperature. This is also comparable to our recent neutron powder diffraction study on samples annealed for weeks [23]: up to 350 °C no significant disorder of Sn on the remaining three cation positions (2a, 2c, 2d) is occurring.

It can be expected that the amount of point defects is increasing with increasing temperature, finally resulting in a statistical distribution of copper, zinc, and tin. As already mentioned, such a high-temperature order-disorder transition was observed by Schorr and Gonzales-Aviles [2], resulting in a cubic sphalerite-type crystal structure.

4. Conclusion

In this work our recently developed mechanochemical synthesis process to phase pure CZTS powder was investigated in more detail. The reaction of the binary sulfides in the ball mill was followed by X-ray diffraction measurements. The crystallite size of the as-milled CZTS powder approaches a value of 10 nm after 3 h of milling. In addition, the crystallization behavior with temperature was investigated by *in situ* high-temperature X-ray diffraction. At 500 °C, $Sn_{Cu/Zn}$ and Cu/Zn_{Sn} anti-site defects are clearly observed. Their concentration strongly decreases when cooling down the

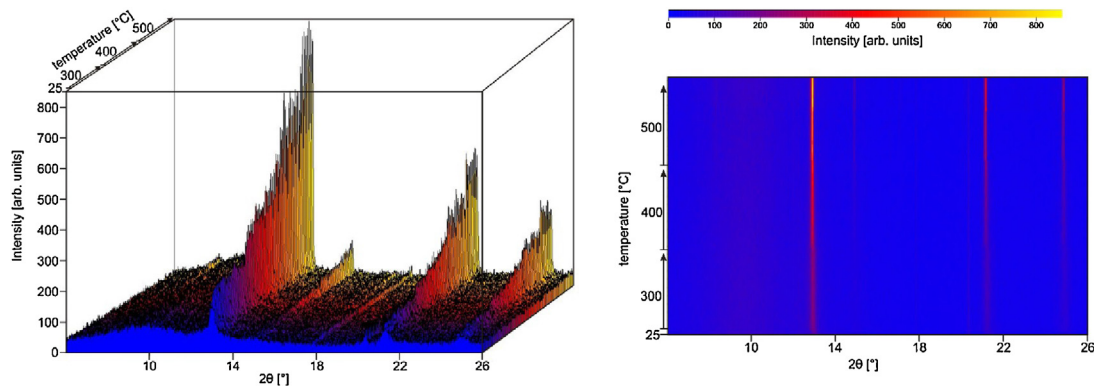


Fig. 5. 3D plot (left) and rainbow contour plot (right) for *in-situ* heat treatment of CZTS precursor powder up to 500 °C (Mo-K α_1 radiation). In the rainbow color contour plot intensities are shown as color scale where low counts are blue, while higher intensities are shown as red and yellow. Temperature increases from the bottom to the top. (For interpretation of the references to colour in this figure legend, the reader is referred to the web version of this article.)

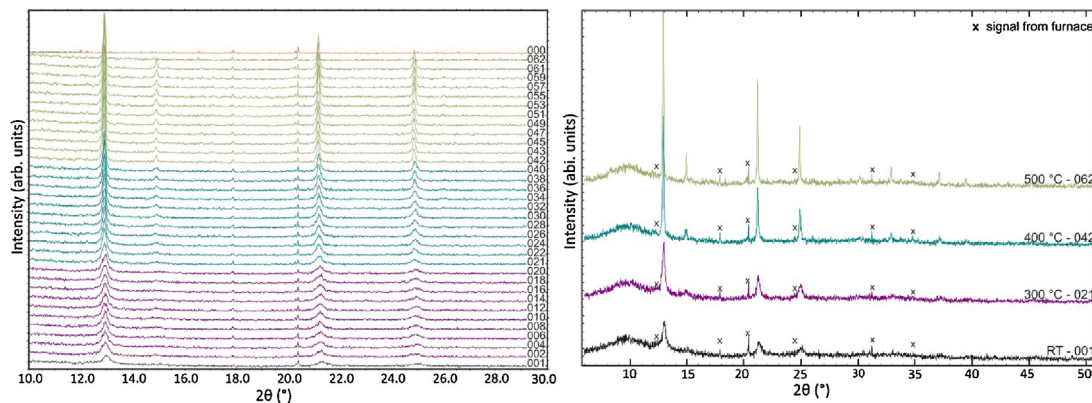


Fig. 6. Evolution of the powder patterns probed by *in situ* high temperature X-ray diffraction (Mo- $K\alpha_1$ radiation). The number of each pattern corresponds to the measurement number N (see experimental section). Pink: 300 °C, blue: 400 °C, green: 500 °C. The starting pattern at 25 °C is shown in black, the pattern of the empty furnace is depicted in orange. (For interpretation of the references to colour in this figure legend, the reader is referred to the web version of this article.)

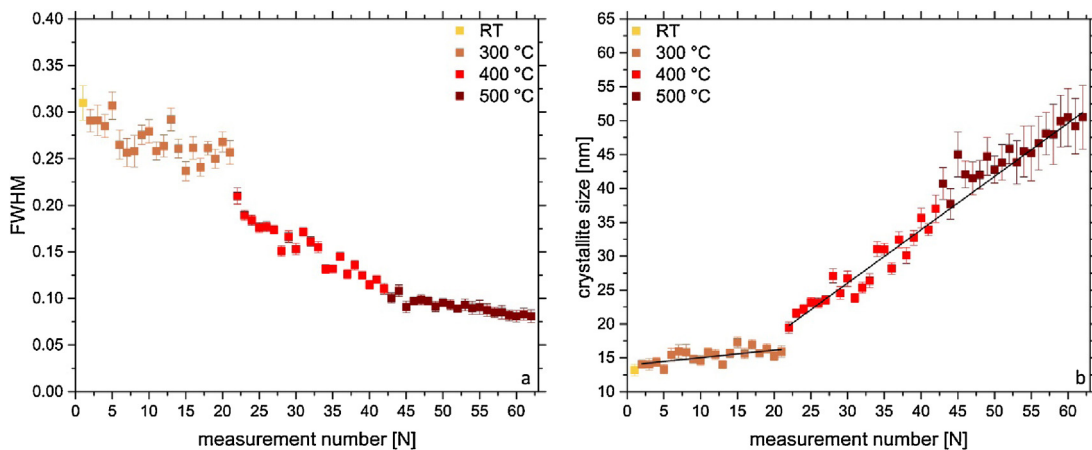


Fig. 7. FWHM values (a) and calculated crystal sizes (b) for the CZTS precursor.

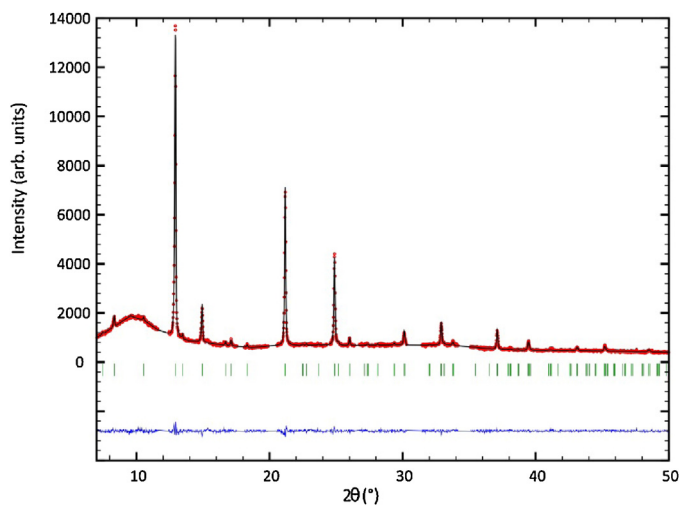


Fig. 8. High temperature (500 °C) X-ray powder diffraction pattern with the results of the Rietveld refinement (excluded regions = signals coming from the furnace).

Table 3
Lattice parameters and residual values of the Rietveld refinement of CZTS at 500 °C.

	X-ray diffraction
Structure type	kesterite
Crystal system	tetragonal
Space group	$I\bar{4}$ (No.82)
Diffractometer	STOE STADI P
Wavelength	70.931 pm
2 θ range	10–50°
T (Measurement)	500 °C
a/pm	546.28(3)
c/pm	1090.10(8)
$R_{\text{Bragg}}/\%$	4.77
$R_{\text{wp}}/\%$	3.84
$R_{\text{exp}}/\%$	3.49
S	1.10

Table 4
Refined structural parameters for CZTS at 500 °C from high temperature X-ray diffraction data.

Atom	Wyckoff	x	y	z	B_{iso}	occ
Cu/Zn	2a	0	0	0	4.00(18)	0.997(11)
Sn	2a	0	0	0	4.00(18)	0.004(11)
Cu/Zn	2c	0	1/2	1/4	4.32(13)	1.000(2)
Sn	2c	0	1/2	1/4	4.32(13)	0.000(2)
Cu/Zn	2d	0	1/2	3/4	4.32(13)	0.922(16)
Sn	2d	0	1/2	3/4	4.32(13)	0.080(16)
Cu/Zn	2b	0	0	1/2	2.36(8)	0.084(11)
Sn	2b	0	0	1/2	2.36(8)	0.918(11)
S	8g	0.748(6)	0.757(5)	0.8699(10)	1.94(9)	4

sample. The cooling rate of 60 K/h seems to be the limit for the production of samples with low Sn-involved disorder, which is important for the performance of CZTS in solar cells. For a more detailed analysis of ordering processes up to the disordered cubic phase, *in situ* high-temperature neutron powder diffraction investigations are planned.

Acknowledgements

Financial support from the MatSEC graduate school of the Helmholtz Zentrum Berlin (HZB) in cooperation with the Dahlem

Research School is gratefully acknowledged. Special thanks to Martin Rohloff (AG Anna Fischer) for performing the TEM measurements.

References

- [1] S. Schorr, H.-J. Hoebler, M. Tovar, Eur. J. Mineral. 19 (2007) 65–73.
- [2] S. Schorr, G. Gonzalez-Aviles, Phys. Status Solidi A 206 (2009) 1054–1058.
- [3] J. Just, D. Luetzenkirchen-Hecht, R. Frahm, S. Schorr, T. Unold, Appl. Phys. Lett. 99 (2011) 262105/1–262105/3.
- [4] S. Chen, X.G. Gong, A. Walsh, S.-H. Wei, Appl. Phys. Lett. 96 (2010) 021902/1–021902/3.
- [5] S. Chen, L.-W. Wang, A. Walsh, X.G. Gong, S.-H. Wei, Appl. Phys. Lett. 101 (2012) 223901/1–223901/4.
- [6] A.J. Jackson, A. Walsh, J. Mater. Chem. A (2014) 7829–7836.
- [7] S. Chen, X.G. Gong, A. Walsh, S.-H. Wei, Appl. Phys. Lett. 94 (2009) 041903/1–041903/3.
- [8] J.J. Scragg, P.J. Dale, L.M. Peter, G. Zoppi, I. Forbes, Phys. Status Solidi B 245 (2008) 1772–1778.
- [9] S. Siebentritt, S. Schorr, Prog. Photovolt. 20 (2012) 512–519.
- [10] W. Wang, M.T. Winkler, O. Gunawan, T. Gokmen, T.K. Todorov, Y. Zhu, D.B. Mitzi, Adv. Energy Mater. 4 (2014) 1301465/1–1301465/5.
- [11] S. Schorr, Sol. Energy Mater. Sol. Cells 95 (2011) 1482–1488.
- [12] L. Choubrac, M. Paris, A. Lafond, C. Guillot-Deudon, X. Rocquefelte, S. Jobic, Phys. Chem. Chem. Phys. 15 (2013) 10722–10725.
- [13] A. Nagoya, R. Asahi, R. Wahl, G. Kresse, Phys. Rev. B Condens. Matter Mater. Phys. 81 (2010) 113202/1–113202/4.
- [14] S. Chen, J.-H. Yang, X.G. Gong, A. Walsh, S.-H. Wei, Phys. Rev. B: Condens. Matter Mater. Phys. 81 (2010) 245204/1–245204/10.
- [15] S. Schorr, M. Tovar, BENSCH Experimental Report, (2006) .
- [16] A. Ritscher, J. Just, O. Dolotko, S. Schorr, M. Lerch, J. Alloys Compd. 670 (2016) 289–296.
- [17] L.E. Valle Rios, K. Neldner, G. Gurieva, S. Schorr, J. Alloys Compd. 657 (2016) 408–413.
- [18] C.F. Burmeister, A. Kwade, Chem. Soc. Rev. 42 (2013) 7660–7667.
- [19] D. Pareek, K.R. Balasubramaniam, P. Sharma, Mater. Charact. 103 (2015) 42–49.
- [20] H.M. Rietveld, J. Appl. Crystallogr. 2 (1969) 65–71.
- [21] J. Rodriguez-Carvajal, Abstracts of the Satellite Meeting on Powder Diffraction of the XV. Congress of the IUCr, 1990, pp. 127.
- [22] P. Scherrer, Nachrichten von der Gesellschaft der Wissenschaften zu Göttingen, Mathematisch-Physikalische Klasse 1918 (1918).
- [23] A. Ritscher, M. Hoelzel, M. Lerch, J. Solid State Chem. 238 (2016) 68–73.
- [24] G. Gurieva, M. Dimitrievska, S. Zander, A. Perez-Rodriguez, V. Izquierdo-Roca, S. Schorr, Phys. Status Solidi C (2015) 1–4.
- [25] A. Lafond, L. Choubrac, C. Guillot-Deudon, P. Deniard, S. Jobic, Z. Anorg. Allg. Chem. 638 (2012) 2571–2577.
- [26] L. Choubrac, A. Lafond, C. Guillot-Deudon, Y. Moelo, S. Jobic, Inorg. Chem. 51 (2012) 3346–3348.
- [27] S. Chen, A. Walsh, X.-G. Gong, S.-H. Wei, Adv. Mater. (Weinheim, Ger.) 25 (2013) 1522–1539.